Proceedings of the ASME 2019
International Design Engineering Technical Conferences
and Computers and Information in Engineering Conference
IDETC/CIE2019
August 18-21, 2019, Anaheim, CA, USA

DETC2019-97551

MODELING AND STABILITY OF MILLING PROCESSES WITH ACTIVE DAMPING

David Lehotzky*
Department of Applied Mechnaics
Budapest University of Technology and Economics
Budapest, Hungary 1111
Email: lehotzky@mm.bme.hu

Zoltan Dombovari
Department of Applied Mechnaics
Budapest University of Technology and Economics
Budapest, Hungary 1111
Email: dombovari@mm.bme.hu

ABSTRACT

In the recent decade, active dampers have been introduced to machining for the avoidance of machine tool chatter in milling processes. The tuning strategy for most of these devices is based on models which do not account for the dynamics of control loop within the active dampers, hence neglect the dynamics of actuator and measuring device, and do not consider filtering. However, these simplified models might lead to inaccurate stability predictions which can deteriorate the performance of active dampers. In order to better approximate the real behavior of milling processes controlled by active dampers, this paper develops a new mathematical model which incorporates the dynamics of control loop within these devices. In particular, the inertial actuator is modeled as an electromagnetic proof-mass transducer, while the dynamics of piezoelectric accelerometer and finite-impulse-response filtering are also taken into account. By the computation of stability lobe diagrams, it is shown that, at low-frequency actuation and at high-speed milling, the consideration of control loop dynamics in active dampers can be essential.

1 INTRODUCTION

Machine tool chatter is a long-studied phenomenon in machining literature. Large-amplitude chatter vibrations can occur between the workpiece and the machined surface due to self-excitation. The so-called regenerative effect [1, 2], modeled by delay-differential equations (DDEs), has provided a commonly accepted explanation for machine tool chatter. Via stability analysis of these DDEs so-called stability lobe diagrams (SLDs) can be computed which depict the regions associated with chatter-free machining in the parameter space of spindle speed and axial depth of cut. Since chatter vibrations are mostly undesired, it has been a subject of great interest how stable domains in SLDs can be increased. Various passive [3, 4], semi-active [5, 6] and active [7, 8] methods have been developed for suppression of machine tool chatter.

Among these, active methods apply controllers which involve feedback loops. The industrial realizations of these controllers all employ discrete sampling and digital data processing. However, in spite of the discrete nature of controllers, most studies assume continuous-time measurements and data processing. Due to the required high computational effort posed by the stability analysis of mathematical models accounting for the discrete nature of control loop, only a few studies [9, 10] have been conducted on this topic, most of them on the turning process. Such studies could reveal whether the neglect of discreteness in the control loop cause changes in SLDs used for tuning of control parameters. Recently, a numerical method [11] has been developed which enables the time-efficient computation of SLDs for such models of milling processes subjected to active damping.

In addition to the neglect of discrete nature in control loop, the tuning strategies for active dampers are based on models which do not consider the full dynamics of control loop of the active damper. These strategies use simplified models to account for the dynamics of actuator and measuring device, and do not consider the discrete nature of filtering. However, these sim-

*Address all correspondence to this author.

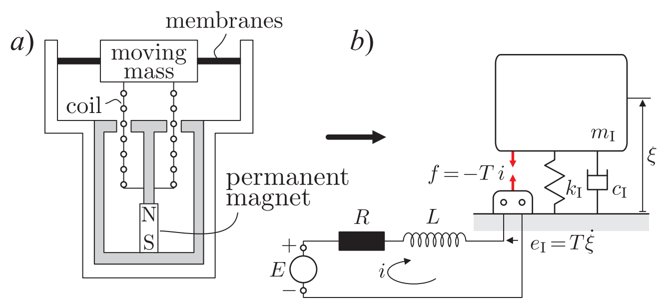

FIGURE 1. Electromechanical model of inertial actuator.

plified models might lead to inaccurate stability predictions that result in a choice of control parameters that brings inferior performance to the active damper. In order to better approximate the real behavior of milling processes subjected to active damping, in this paper we develop a new mathematical model which takes into account the dynamics of control loop in more detail. We model the active damper as an electromechanical proof-mass transducer, incorporate the dynamics of piezoelectric accelerometer and take into account finite-impulse-response filtering rules applied to the output signal of accelerometer. By computation of SLDs, we show that at low-frequency actuation and at high-speed milling a more precise modeling of the control loop dynamics can be essential for the efficient tuning of active dampers.

2 MODELING

This section presents the step-by-step construction of the mathematical model. For clarity, the modeling of actuator, accelerometer, milling process, cutting force and filtering are described in separate subsections.

2.1 Actuator

In this study, we assume that the active damper is an inertial (proof-mass) actuator which is modeled according to Chapter 3.2.1 in [12]. This subsection presents the subsystem of actuator which is later integrated into the model of milling in Section 2.3. Fig. 1 shows the electromechanical model of a proof-mass actuator fixed to rigid support. The Newtonian equation, governing the mechanical part of the model is

$$m_\mathrm{I}\ddot{\xi}(t)+c_\mathrm{I}\dot{\xi}(t)+k_\mathrm{I}\xi(t)=-f(t), \tag{1}$$

where m_I, c_I and k_I are the mass, damping and stiffness of inertial actuator, respectively. The Laplace force induced by the electromagnetic field is denoted by $f(t)=-Ti(t)$, where T is the transducer constant and $i(t)$ is the electric current of the actuator. The governing equation of the electric circuit reads as

TABLE 1. PARAMETERS OF INERTIAL ACTUATOR FROM TAB. 2 IN [13].

Parameter	Notation	Value	Unit
moving mass	m_I	1.35	[kg]
damping ratio	ζ_I	0.05	[1]
natural angular frequency	ω_I	$2\pi\times 40$	[rad/s]
transducer constant	T	5.6	[N/A]
resistance	R	1.7	[Ω]
inductance	L	0.298×10^{-3}	[H]

$$e_\mathrm{I}(t)+L\frac{\mathrm{d}i(t)}{\mathrm{d}t}+Ri(t)=E(t), \tag{2}$$

where L is the inductance and R is the resistance of coil. Voltage source $E(t)$ moves current along the circuit, and according to Faraday's law, the voltage between the circuit's two end is $e_\mathrm{I}(t)=T\dot{\xi}(t)$. The total force, applied to the support is

$$Q(t)=-m_\mathrm{I}\ddot{\xi}(t). \tag{3}$$

Using Eqns. (1)–(3), the transfer function between voltage input $E(t)$ and force output $Q(t)$ can be expressed in the Laplace domain as

$$G_\mathrm{I}(s)=\frac{Q(s)}{E(s)}=-\frac{s^2}{\left(\omega_\mathrm{I}^2+2\zeta_\mathrm{I}\omega_\mathrm{I}s+s^2\right)\left(\tilde{R}+\tilde{L}s\right)+s\tilde{m}_\mathrm{I}^{-1}}, \tag{4}$$

where $\omega_\mathrm{I}=\sqrt{k_\mathrm{I}/m_\mathrm{I}}$ is the natural angular frequency and $\zeta_\mathrm{I}=c_\mathrm{I}/(2m_\mathrm{I}\omega_\mathrm{I})$ is the damping ratio of the inertial actuator, while $\tilde{R}=R/T$, $\tilde{L}=L/T$ and $\tilde{m}_\mathrm{I}=m_\mathrm{I}/T$ denote the specific resistance, inductance and mass of the inertial actuator, respectively. For the typical parameter setting specified in Tab. 1, the magnitude and phase plots of $G_\mathrm{I}(\mathrm{i}\omega)$ are shown in Fig. 2 with red color.

Simplification I. With the neglect of inductance L and assuming current instead of voltage generator, the governing equation Eqn. (2) of the electric circuit can be omitted and using Eqn. (1) and Eqn. (3), the transfer function between voltage

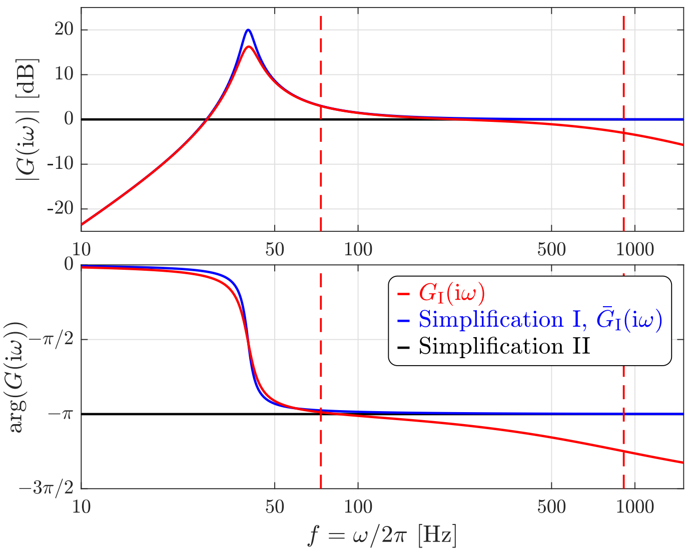

FIGURE 2. Magnitude and phase shift of the transfer function of inertial actuator subjected to different simplifications and using parameters from Tab. 1. The magnitude plot is shifted to the nominal transmission coefficient of ideal force generator (marked by black line). The red dashed lines mark cutoff frequencies corresponding to ±3 dB differences in magnitude from the nominal transmission coefficient.

input and force output becomes

$$\bar{G}_{\mathrm{I}}(s)=\frac{Q(s)}{Ri(s)}=-\frac{\tilde{R}^{-1}s^2}{\omega_{\mathrm{I}}^2+2\zeta_{\mathrm{I}}\omega_{\mathrm{I}}s+s^2} \tag{5}$$

This is a common assumption used during the modeling of inertial actuators [14–16]. Note that by assuming large $\tilde{m}_{\mathrm{I}}$ and small $\tilde{L}$, $G_{\mathrm{I}}(s)\approx\bar{G}_{\mathrm{I}}(s)$. For the typical parameter setting specified in Tab. 1, the magnitude and phase plots of $\bar{G}_{\mathrm{I}}(\mathrm{i}\omega)$ are shown in Fig. 2 with blue color.

Simplification II. Note that for small $\tilde{L}$ and large s (that is for high frequencies) $|G_{\mathrm{I}}(s)|\approx\left|\bar{G}_{\mathrm{I}}(s)\right|\approx\tilde{R}^{-1}$, therefore at high frequencies the actuator behaves like an ideal force generator. This is also a common assumption in the literature [8, 17].

As references [8, 14–17] show, the herein presented two simplifications are widespread in the machining literature for inertial actuator models. In order to see the effect of such simplifications on stability of the general model, developed in this paper, we compare the results obtained with and without the above described simplifications.

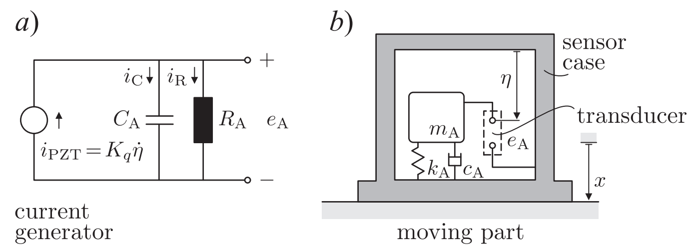

FIGURE 3. Electromechanical model of piezoelectric accelerometer.

2.2 Accelerometer

Most mathematical models of control systems involving acceleration feedback assume ideal measurements of the acceleration signal without accounting for the dynamics of measuring device. Here we incorporate the piezoelectric accelerometer in the mathematical model of the actively damped milling process. This is done in order to see how the neglect of the dynamics of accelerometer affects the results for stability. This subsection presents the subsystem of piezoelectric accelerometer adopted from [18]. This subsystem is integrated into the model of milling in Section 2.3.

The mechanical model of the piezoelectric accelerometer is shown in Fig. 3/b. The governing equation of the seismic mass m_{A} can be easily derived using Newtonian mechanics, it reads as

$$-m_{\mathrm{A}}\left(\ddot{x}(t)+\ddot{\eta}(t)\right)=k_{\mathrm{A}}\eta(t)+c_{\mathrm{A}}\dot{\eta}(t), \tag{6}$$

where k_{A} and c_{A} are the stiffness and damping coefficients, respectively between the case and seismic mass. Coordinate x is measured in a steady frame of reference and it locates the sensor case fixed to a moving part. Coordinate η gives the position of seismic mass relative to the case, measured from the position of seismic mass under no motion (that is from the steady position of seismic mass). Governing equation Eqn. (6) can be rearranged as

$$\ddot{\eta}(t)=-\omega_{\mathrm{A}}^2\eta(t)-2\zeta_{\mathrm{A}}\omega_{\mathrm{A}}\dot{\eta}(t)-\ddot{x}(t), \tag{7}$$

with $\omega_{\mathrm{A}}=\sqrt{k_{\mathrm{A}}/m_{\mathrm{A}}}$ and $\zeta_{\mathrm{A}}=c_{\mathrm{A}}/(2m_{\mathrm{A}}\omega_{\mathrm{A}})$ being the natural angular frequency and damping ratio of seismic mass, respectively. The piezoelectric transducer of the sensor assumes a linear relationship between the output charge q and the displacement of seismic mass η in the form $q(t)=K_q\eta(t)$, where K_q is the charge output of unit displacement. The piezoelectric subsystem can be modeled by the equivalent circuit shown in Fig. 3/a (for more details, see [18]), where charge generated due to displacement of seismic mass is included in the current generator $i_{\mathrm{PZT}}(t)=\dot{q}(t)$. The equivalent capacity of wiring, amplifier and

TABLE 2. PARAMETERS OF ACCELEROMETER BRÜEL & KJÆR VIBRO AS–022.

Parameter	Notation	Value	Unit
seismic mass	m_{A}	0.05	[kg]
damping ratio	ζ_{A}	0.02	[1]
natural angular frequency	ω_{A}	$2\pi\times35\times10^3$	[rad/s]
electric sensitivity	S_{e}	4.9328×10^5	[V/m]
electric time constant	τ_{A}	0.1194	[s]

transducer is denoted by C_{A}, while R_{A} is the equivalent resistance of amplifier and transducer. The voltage measured on the transducer is denoted by $e_{\mathrm{A}}(t)$. According to Kirchoff's current law $-i_{\mathrm{PZT}}(t)+i_{\mathrm{C}}(t)+i_{\mathrm{R}}(t)=0$, which after applying Ohm's law gives

$$\dot{e}_{\mathrm{A}}(t)=S_{\mathrm{e}}\dot{\eta}(t)-\frac{1}{\tau_{\mathrm{A}}}e_{\mathrm{A}}(t), \tag{8}$$

where $S_{\mathrm{e}}=K_q/C_{\mathrm{A}}$ is the electric sensitivity of piezoelectric accelerometer, while $\tau_{\mathrm{A}}=R_{\mathrm{A}}C_{\mathrm{A}}$ is the electric time constant. Together, Eqn. (7) and Eqn. (8) form the system of governing equations for the piezoelectric accelerometer. The transfer function between input acceleration $\ddot{x}(t)$ and output voltage $e_{\mathrm{A}}(t)$ can be expressed from Eqns. (7)–(8) in the Laplace domain as

$$G_{\mathrm{A}}(s)=\frac{e_{\mathrm{A}}(s)}{s^2x(s)}=-S_{\mathrm{T}}\frac{\tau_{\mathrm{A}}s}{\tau_{\mathrm{A}}s+1}\frac{\omega_{\mathrm{A}}^2}{s^2+2\zeta_{\mathrm{A}}\omega_{\mathrm{A}}s+\omega_{\mathrm{A}}^2}, \tag{9}$$

where $S_{\mathrm{T}}=S_{\mathrm{m}}S_{\mathrm{e}}$ is the sensor sensitivity, with $S_{\mathrm{m}}=1/\omega_{\mathrm{A}}^2$ being the mechanical sensitivity.

Simplification III. The magnitude and phase plots of transfer function $G_{\mathrm{A}}(\mathrm{i}\omega)$ are shown in Fig. 4 for the typical parameter setting given in Tab. 2. As Fig. 4 illustrates, the transfer function of piezoelectric accelerometer has a constant magnitude and an almost-constant shift in a wide frequency domain. This is the frequency range of measurement. Given this characteristic of the transfer function, it is a common assumption that the dynamics of piezoelectric accelerometer does not need to be incorporated in the mathematical model. However, this simplification might leads to error in stability computations therefore its effect is investigated within this paper.

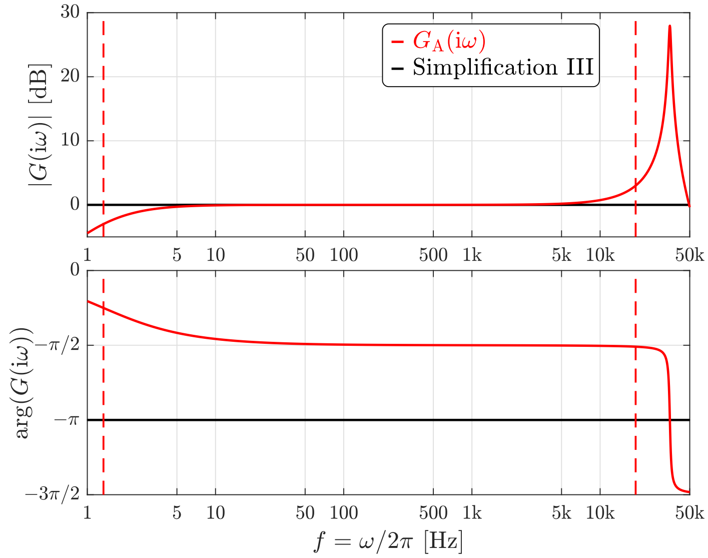

FIGURE 4. Magnitude and phase shift of the transfer function of piezoelectric accelerometer using parameters from Tab. 2. The magnitude plot is shifted to the nominal transmission coefficient corresponding to ideal relationship between output voltage $e_{\mathrm{A}}(t)$ and input acceleration $\ddot{x}(t)$. The red dashed lines mark cutoff frequencies corresponding to ±3 dB differences in magnitude from the nominal transmission coefficient.

2.3 Milling process

A simplified model of milling with active damping is shown in Fig. 5. It is assumed that the cutting tool can be represented at point P with a single modal mass m, modal stiffness k and modal damping coefficient c corresponding to direction X. The displacement of center point P of the cutting end of the tool is measured with respect to a steady frame using coordinate x. Note that, in general, milling cannot be modeled using a single mode and the modal direction does not coincide with that of the feed velocity $\mathbf{v}_{\mathrm{f}}$ (see e.g. [19]). However, in order to focus the attention on modeling of active damper, only a single mode is taken into account whose direction is parallel to $\mathbf{v}_{\mathrm{f}}$. Consequently, the vibration of cutting tool is neglected in directions perpendicular to the feed velocity $\mathbf{v}_{\mathrm{f}}$. It is assumed that, as Fig. 5 indicates, the piezoelectric accelerometer and inertial actuator are assembled on opposite sides of the cutting tool at point R. It is also assumed that point R is close-enough to point P such that the motion of point R can be directly given by x. Here we note that the effect of points P and R being non-collocated might deserves attention in future studies. The voltage signal $e_{\mathrm{A}}(t)$ of accelerometer is processed by a finite impulse response (FIR) filter, then after the application of a control law it is fed back to the voltage signal $E(t)$ of inertial actuator. The modeling of FIR filtering and control law are addressed in Section 2.5. The displacement of seismic

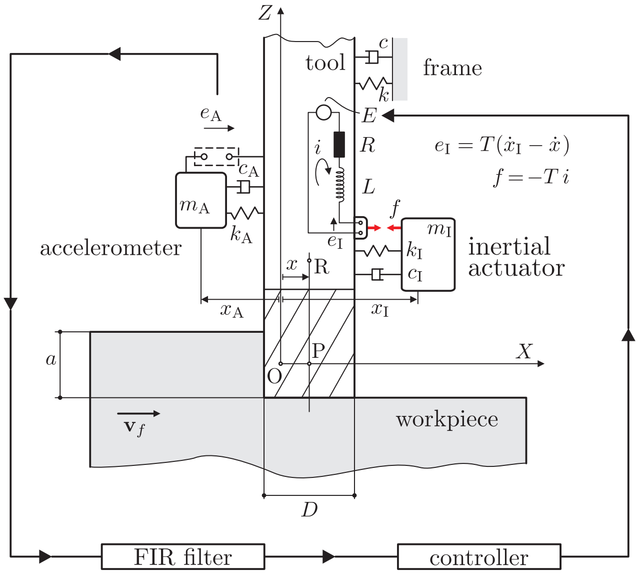

FIGURE 5. Model of milling process subjected to active damping.

mass m_A and moving mass m_I are denoted by x_A, and x_I, respectively, both in the steady reference frame. Governing equations for the model shown in Fig. 5 can be derived using a Lagrangian approach with the inclusion of Eqn. (2) and Eqn. (8), that is the circuit equations of actuator and accelerometer. Choosing the vector of general coordinates as $\mathbf{q} = [x \;\; \xi \;\; \eta]^\mathsf{T}$ with $\xi = x_I - x$ and $\eta = -x - x_A$, the Lagrangian equation of motion of 2nd kind reads as

$$\mathbf{M}\ddot{\mathbf{q}}(t) + \mathbf{C}\dot{\mathbf{q}}(t) + \mathbf{K}\mathbf{q}(t) = \mathbf{F}(t), \tag{10}$$

where coefficient matrices are

$$\mathbf{M} = \begin{bmatrix} m+m_I+m_A & m_I & m_A \\ m_I & m_I & 0 \\ m_A & 0 & m_A \end{bmatrix}, \tag{11}$$

$$\mathbf{C} = \begin{bmatrix} c & 0 & 0 \\ 0 & c_I & 0 \\ 0 & 0 & c_A \end{bmatrix}, \mathbf{K} = \begin{bmatrix} k & 0 & 0 \\ 0 & k_I & 0 \\ 0 & 0 & k_A \end{bmatrix}, \tag{12}$$

and the force vector is

$$\mathbf{F}(t) = \left[F(t) \;\; -f(t) \;\; 0 \right]^\mathsf{T}, \tag{13}$$

with $F(t)$ being the horizontal cutting force acting on the tool. Formulas used for the cutting force are detailed in Section 2.4. After attaching circuit equations Eqn. (2) and Eqn. (8) to the first-order form of Eqn. (10), furthermore by normalizing time according to $\hat{t} = \omega_n t$, with $\omega_n = \sqrt{k/m}$ and dropping the hat immediately, the governing equation reads as

$$\dot{\mathbf{z}}(t) = \mathbf{A}\mathbf{z}(t) + \mathbf{b}F(t) + \mathbf{d}E(t), \tag{14}$$

where the state vector is $\mathbf{z}(t) = [\mathbf{q}^\mathsf{T}(t) \; \dot{\mathbf{q}}^\mathsf{T}(t) \; i(t) \; e_A(t)]^\mathsf{T}$ and coefficient matrices are

$$\mathbf{A} = \begin{bmatrix} \underset{(3\times3)}{\mathbf{0}} & \underset{(3\times3)}{\mathbf{I}} & \underset{(3\times1)}{\mathbf{0}} & \underset{(3\times1)}{\mathbf{0}} \\ -\tilde{\mathbf{K}} & -\tilde{\mathbf{C}} & \tilde{\mathbf{Q}}_I & \underset{(3\times1)}{\mathbf{0}} \\ \underset{(2\times3)}{\mathbf{0}} & \mathbf{E} & \mathbf{E}_I & \mathbf{E}_A \end{bmatrix}, \mathbf{b} = \begin{bmatrix} \underset{(3\times1)}{\mathbf{0}} \\ \tilde{\mathbf{Q}}_c \\ \underset{(2\times1)}{\mathbf{0}} \end{bmatrix}, \mathbf{d} = \begin{bmatrix} \underset{(6\times1)}{\mathbf{0}} \\ \frac{1}{\omega_n L} \\ 0 \end{bmatrix}, \tag{15}$$

with $\underset{(\alpha\times\beta)}{\mathbf{0}}$ and $\underset{(\alpha\times\beta)}{\mathbf{I}}$ being zero and identity matrices, respectively of size $\alpha \times \beta$. Other coefficient sub-matrices are

$$\tilde{\mathbf{K}} = \frac{1}{\omega_n^2}\mathbf{M}^{-1}\mathbf{K} = \begin{bmatrix} 1 & -\nu_I & -\nu_A \\ -1 & \nu_I(1+\mu_I) & \nu_A \\ -1 & \nu_I & \nu_A(1+\mu_A) \end{bmatrix}, \tag{16}$$

$$\tilde{\mathbf{C}} = \frac{1}{\omega_n}\mathbf{M}^{-1}\mathbf{C} = 2\zeta \begin{bmatrix} 1 & -\delta_I & -\delta_A \\ -1 & \delta_I(1+\mu_I) & \delta_A \\ -1 & \delta_I & \delta_A(1+\mu_A) \end{bmatrix}, \tag{17}$$

$$\tilde{\mathbf{Q}}_I = \frac{1}{\omega_n^2}\mathbf{M}^{-1}\begin{bmatrix} 0 \\ T \\ 0 \end{bmatrix} = \frac{T}{\hat{m}}\begin{bmatrix} -1 \\ 1+\mu_I \\ 1 \end{bmatrix}, \tag{18}$$

$$\tilde{\mathbf{Q}}_c = \frac{1}{\omega_n^2}\mathbf{M}^{-1}\begin{bmatrix} 1 \\ 0 \\ 0 \end{bmatrix} = \frac{1}{\hat{m}}\begin{bmatrix} 1 \\ -1 \\ -1 \end{bmatrix}, \tag{19}$$

$$\mathbf{E} = \begin{bmatrix} 0 & -T/L & 0 \\ 0 & 0 & S_e \end{bmatrix}, \mathbf{E}_I = \begin{bmatrix} -\hat{R}/L \\ 0 \end{bmatrix}, \mathbf{E}_A = \begin{bmatrix} 0 \\ -1/\hat{\tau}_A \end{bmatrix}, \tag{20}$$

where ω_n is the natural angular frequency and $\zeta = c/(2m\omega_n)$ is the damping ratio corresponding to the horizontal mode of the tool, $\nu_I = k_I/k$, $\nu_A = k_A/k$ are the stiffness ratios, $\mu_I = m/m_I$ and $\mu_A = m/m_A$ are the mass ratios, while $\delta_I = c_I/c$ and $\delta_A = c_A/c$ are the damping coefficient ratios. The normalized modal mass is $\hat{m} = m\omega_n^2$, the normalized resistance is denoted by $\hat{R} = R/\omega_n$ and the dimensionless electric time constant is $\hat{\tau}_A = \tau_A\omega_n$.

Changes in the governing equation Eqn. (14), due to simplifications detailed under Sections 2.1–2.2, are discussed below.

Simplification I. This simplification omits the dynamics of electric circuit in the inertial actuator, which results in $i(t) = E(t)/R$ and leads to a governing equation formally equivalent to

Eqn. (14), where the state vector is $\mathbf{z}(t) = [\mathbf{q}^\mathsf{T}(t)\ \dot{\mathbf{q}}^\mathsf{T}(t)\ e_\mathrm{A}(t)]^\mathsf{T}$ and coefficient matrices are

$$\mathbf{A} = \begin{bmatrix} \underset{(3\times3)}{\mathbf{0}} & \underset{(3\times3)}{\mathbf{I}} & \underset{(3\times1)}{\mathbf{0}} \\ -\tilde{\mathbf{K}} & -\tilde{\mathbf{C}} & \underset{(3\times1)}{\mathbf{0}} \\ \underset{(1\times3)}{\mathbf{0}} & \mathbf{E}_1 & -1/\hat{\tau}_\mathrm{A} \end{bmatrix}, \mathbf{b} = \begin{bmatrix} \underset{(3\times1)}{\mathbf{0}} \\ \tilde{\mathbf{Q}}_\mathrm{c} \\ 0 \end{bmatrix}, \mathbf{d} = \frac{1}{R}\begin{bmatrix} \underset{(3\times1)}{\mathbf{0}} \\ \tilde{\mathbf{Q}}_\mathrm{I} \\ 0 \end{bmatrix}, \quad (21)$$

with sub-matrices defined according to Eqns. (16)–(20) and $\mathbf{E}_1 = [0\ \ 0\ \ S_\mathrm{e}]$.

Simplification II. This simplification leads to an ideal force generator with the constant linear relationship $Q(t) = -E(t)/\tilde{R}$ between force output $Q(t)$ and input voltage $E(t)$ of the inertial actuator. The resulting governing equation takes the form of Eqn. (14), where the state vector is $\mathbf{z}(t) = [\mathbf{q}^\mathsf{T}(t)\ \dot{\mathbf{q}}^\mathsf{T}(t)\ e_\mathrm{A}(t)]^\mathsf{T}$, with general coordinates $\mathbf{q} = [x\ \ \eta]^\mathsf{T}$. Now the coefficient matrices of Eqn. (14) are

$$\mathbf{A} = \begin{bmatrix} \underset{(2\times2)}{\mathbf{0}} & \underset{(2\times2)}{\mathbf{I}} & \underset{(2\times1)}{\mathbf{0}} \\ -\tilde{\mathbf{K}}_2 & -\tilde{\mathbf{C}}_2 & \underset{(2\times1)}{\mathbf{0}} \\ \underset{(1\times2)}{\mathbf{0}} & \mathbf{E}_2 & -1/\hat{\tau}_\mathrm{A} \end{bmatrix}, \mathbf{b} = \begin{bmatrix} \underset{(2\times1)}{\mathbf{0}} \\ \tilde{\mathbf{Q}}_{\mathrm{c},2} \\ 0 \end{bmatrix}, \mathbf{d} = \begin{bmatrix} \underset{(2\times1)}{\mathbf{0}} \\ \tilde{\mathbf{Q}}_{\mathrm{I},2} \\ 0 \end{bmatrix}, \quad (22)$$

with sub-matrices

$$\tilde{\mathbf{K}}_2 = \begin{bmatrix} 1 & -\nu_\mathrm{A} \\ -1 & \nu_\mathrm{A}(1+\mu_\mathrm{A}) \end{bmatrix}, \tilde{\mathbf{C}}_2 = 2\zeta \begin{bmatrix} 1 & -\delta_\mathrm{A} \\ -1 & \delta_\mathrm{A}(1+\mu_\mathrm{A}) \end{bmatrix}, \quad (23)$$

$$\tilde{\mathbf{Q}}_{\mathrm{I},2} = \frac{T}{R\hat{m}}\begin{bmatrix} -1 \\ 1 \end{bmatrix}, \tilde{\mathbf{Q}}_{\mathrm{c},2} = \frac{1}{\hat{m}}\begin{bmatrix} 1 \\ -1 \end{bmatrix}, \mathbf{E}_2 = [0\ \ S_\mathrm{e}]. \quad (24)$$

Simplification III. Ideal relationship between the measured accelerometer output voltage $e_\mathrm{A}(t)$ and input acceleration $\ddot{x}(t)$ is assumed by this simplification. This leads to the omission of seismic mass dynamics and corresponding electric circuit dynamics from the governing equation Eqn. (14), where the state vector is $\mathbf{z}(t) = [\mathbf{q}^\mathsf{T}(t)\ \dot{\mathbf{q}}^\mathsf{T}(t)\ i(t)]^\mathsf{T}$, with general coordinates $\mathbf{q} = [x\ \ \xi]^\mathsf{T}$. Now the coefficient matrices of Eqn. (14) are

$$\mathbf{A} = \begin{bmatrix} \underset{(2\times2)}{\mathbf{0}} & \underset{(2\times2)}{\mathbf{I}} & \underset{(2\times1)}{\mathbf{0}} \\ -\tilde{\mathbf{K}}_3 & -\tilde{\mathbf{C}}_3 & \tilde{\mathbf{Q}}_{\mathrm{I},3} \\ \underset{(1\times2)}{\mathbf{0}} & \mathbf{E}_3 & -\hat{R}/L \end{bmatrix}, \mathbf{b} = \begin{bmatrix} \underset{(2\times1)}{\mathbf{0}} \\ \tilde{\mathbf{Q}}_{\mathrm{c},2} \\ 0 \end{bmatrix}, \mathbf{d} = \begin{bmatrix} \underset{(4\times1)}{\mathbf{0}} \\ \frac{1}{\omega_\mathrm{n} L} \end{bmatrix}, \quad (25)$$

with sub-matrices defined according to Eqn. (24) and

$$\tilde{\mathbf{K}}_3 = \begin{bmatrix} 1 & -\nu_\mathrm{I} \\ -1 & \nu_\mathrm{I}(1+\mu_\mathrm{I}) \end{bmatrix}, \tilde{\mathbf{C}}_3 = 2\zeta \begin{bmatrix} 1 & -\delta_\mathrm{I} \\ -1 & \delta_\mathrm{I}(1+\mu_\mathrm{I}) \end{bmatrix}, \quad (26)$$

$$\tilde{\mathbf{Q}}_{\mathrm{I},3} = \frac{T}{\hat{m}}\begin{bmatrix} -1 \\ 1+\mu_\mathrm{I} \end{bmatrix}, \mathbf{E}_3 = [0\ \ -T/L]. \quad (27)$$

2.4 Cutting force

In this study we assume that the cutting force on each cutting teeth can be computed according to the linear formula

$$\underset{(t,r)}{\mathbf{F}_p}(t) = \begin{bmatrix} K_\mathrm{t} \\ K_\mathrm{n} \end{bmatrix} a h_p(t), \quad p = 1,\ldots,Z; \quad (28)$$

where a is the axial depth of cut, h_p is the chip thickness on the p-th tooth, K_t and K_n are the tangential and normal cutting force coefficients, respectively and Z is the number of cutting teeth. It worths mention that other formulas have also been used in machining literature for modeling of cutting force, a good summary can be found in Fig. 1 of [20].

Although more accurate formulas for the chip thickness can also be found in the literature (see e.g. [21–23]), here we limit our attention only to the effect of active damping and employ the widespread circular tooth path approximation (for details on this approximation, see Chapter 5.2.4 in [24]). After introducing normalized time $\hat{t} = \omega_\mathrm{n} t$ and dropping the hat immediately, furthermore with the neglect of vibrations perpendicular to the feed velocity, the circular tooth path approximation gives

$$h_p(t) \approx (f_\mathrm{Z} + x(t-\hat{\tau}) - x(t))\sin\varphi_p(t), \quad (29)$$

where $f_Z = \hat{v}_\mathrm{f}\hat{\tau}$ is the feed rate, with $\hat{v}_\mathrm{f} = v_\mathrm{f}/\omega_\mathrm{n}$ being the normalized feed rate. The normalized tooth pass period is denoted by $\hat{\tau} = \omega_\mathrm{n}\tau$, with $\tau = 60/(\Omega Z)$ being the tooth pass period. The normalized spindle speed is $\hat{\Omega} = 2\pi\Omega Z/(60\omega_\mathrm{n})$, with Ω being the spindle speed in [rpm]. The angular position of each tooth is given according to $\varphi_p(t) = (\hat{\Omega}t + (p-1)2\pi)/Z$.

Note that in Eqn. (28), $\mathbf{F}_p$ is given in the tangential-radial (t,r) coordinate system. After transformation to the steady (X,Y) coordinate system, the resultant cutting force vector is given by

$$\underset{(X,Y)}{\mathbf{F}_\mathrm{c}}(t) = \sum_{p=1}^{Z} g_p(t)\mathbf{T}_p(t)\underset{(t,r)}{\mathbf{F}_p}(t), \quad (30)$$

where matrix

$$\mathbf{T}_p(t) = \begin{bmatrix} \cos\varphi_p(t) & \sin\varphi_p(t) \\ -\sin\varphi_p(t) & \cos\varphi_p(t) \end{bmatrix}, \quad (31)$$

transforms cutting force Eqn. (28) to the (X,Y) coordinate system and window function

$$g_p(t)=\begin{cases}1 & \text{if } \varphi_{\text{ent}}\leq \varphi_p(t) \bmod 2\pi \leq \varphi_{\text{ex}},\\ 0 & \text{otherwise,}\end{cases} \tag{32}$$

accounts for whether the p-th tooth is in or out of the cut. Here φ_{ent} and φ_{ex} stand for the entrance and exit angles. For up-milling operation $\varphi_{\text{ent}}=0$ and $\varphi_{\text{ex}}=\arccos(1-2a_{\text{e}}/D)$, where a_{e} is the radial immersion and D is the diameter of cutting tool (see Fig. 5). For down-milling operation $\varphi_{\text{ent}}=\arccos(2a_{\text{e}}/D-1)$ and $\varphi_{\text{ex}}=\pi$. Note that, due to the neglect of vibrations perpendicular to $\mathbf{v}_{\text{f}}$, only the horizontal component of cutting force $\mathbf{F}_{\text{c}}$ is of interest to us. From Eqn. (30), this component reads as

$$F\left(t,x,x(t-\hat{\tau})\right)=F_0(t)+H(t)\left(x(t-\hat{\tau})-x(t)\right), \tag{33}$$

where

$$F_0(t)=af_Z\sum_{p=1}^{Z}g(t)\left(K_{\text{n}}\sin\varphi_p(t)+K_{\text{t}}\cos\varphi_p(t)\right) \tag{34}$$

$$H(t)=a\sum_{p=1}^{Z}g(t)\left(K_{\text{n}}\sin\varphi_p(t)+K_{\text{t}}\cos\varphi_p(t)\right)\sin\varphi_p(t) \tag{35}$$

are the state-independent part of horizontal cutting force and the time-periodic cutting force coefficient, respectively.

2.5 Filtering and control

The overwhelming majority of studies in the machining literature assume continuous actuator signal (see e.g. [8, 15, 16]). In addition, many of them do not account for the time delay between measurement and actuation (see e.g. [8, 15]). However, in reality, the actuator input is piecewise-constant and there is time lag between the measured signal and the computed input of the actuator due to data processing. In this paper, we account for all these factors in order to see how the continuous and delay-free actuator signal assumptions affect the stability of actively damped milling processes.

It is assumed that the output voltage signal $e_{\text{A}}(t)$ of accelerometer is sampled with frequency f_{s}. We employ velocity feedback control, which is intended to provide artificial damping to the milling process. Consequently, the acceleration signal is numerically integrated, and its value is updated upon the arrival of new accelerometer output voltage samples. This results in the piecewise-constant velocity signal

$$v(t)=v_i,\quad \left[t_i,t_{i+1}\right), \tag{36}$$

where the rectangle rule

$$v_i=v_{i-1}+\frac{\Delta t}{S_{\text{T}}}e_{\text{A}}\left(t_i-r_{\text{int}}\Delta t\right) \tag{37}$$

is applied for integration. Here $i\in\mathbb{N}$, $\Delta t=t_{i+1}-t_i=1/f_{\text{s}}$ is the sampling period, and $r_{\text{int}}\Delta t$ is the time demand of integration, with $r_{\text{int}}\in\mathbb{Z}^+$. The velocity signal is passed through a FIR filter of order N, which uses $N+1$ number of the most recent velocity values. Consequently, after filtering, the velocity signal reads as

$$v_{\text{FIR}}(t)=\sum_{r=0}^{N}c_r\,v(t-(r+r_{\text{FIR}})\Delta t) \tag{38}$$

where c_r are the FIR filter coefficients and the time demand $r_{\text{FIR}}\Delta t$ of filtering is assumed to be an integer $r_{\text{FIR}}\in\mathbb{Z}^+$ multiple of the sampling period. The filtered velocity signal (38) is fed back to the actuator input voltage according to

$$E(t)=G\,v_{\text{FIR}}(t_j),\quad \left[t_j,t_{j+1}\right), \tag{39}$$

with velocity feedback gain G. This formula assumes zero-order hold of the actuator input signal: $E(t)$ is updated at $t_j=j\Delta T$ time instants, and it is kept constant between two subsequent updates. We assume that the actuation period $\Delta T=\kappa\Delta t$ is a positive integer $\kappa\in\mathbb{Z}^+$ multiple of the sampling period. After rescaling time according to $\hat{t}=\omega_{\text{n}}t$ and dropping the hat immediately, $E(t)$ can be expressed from Eqns. (36)–(39) as

$$E(t)=E_j,\quad t\in\left[t_j,t_j+\Delta\hat{T}\right), \tag{40}$$

$$E_j=E_{j-1}+\sum_{r=0}^{N+1}C_r\sum_{k=0}^{\kappa-1}e_{\text{A}}\left(t_j-\left(r+r_{\text{p}}-k\right)\Delta\hat{t}\right), \tag{41}$$

where $r_{\text{p}}=r_{\text{int}}+r_{\text{FIR}}$, with $r_{\text{p}}\Delta t$ being the overall delay due to data processing. The dimensionless feedback coefficients are $C_r=(\tilde{G}\Delta\hat{t}c_r)/S_{\text{T}}$, where $\tilde{G}=G/\omega_{\text{n}}$ is the normalized velocity feedback gain and $\Delta\hat{t}=\omega_{\text{n}}\Delta t$ is the dimensionless sampling period. The dimensionless actuation period is $\Delta\hat{T}=\omega_{\text{n}}\Delta T$.

Specifications In order to avoid the resonance of seismic mass in accelerometer, the sampling frequency is set below the upper cutoff frequency ($\approx 18\times10^3$ [Hz]) of the accelerometer: $f_{\text{s}}=18\times10^3$ [Hz].

In order to attenuate lower frequencies amplified by integration and to avoid resonant frequencies of the actuator, a high-pass

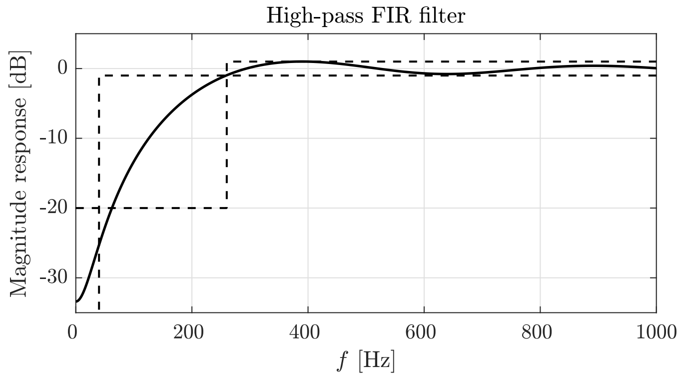

FIGURE 6. Magnitude response function of FIR filter applied to velocity signal $v(t)$ in Eqn. (38). The filter was designed in Matlab, using Kaiser window. Design specifications are listed in Tab. 3. The passband and stopband frequencies, the limits for passband ripple and the stopband attenuation are illustrated with dashed lines.

TABLE 3. PARAMETERS OF HIGH-PASS FIR FILTER

Parameters	Value	Unit
stopband frequency	40	[Hz]
passband frequency	260	[Hz]
passband ripple	2	[dB]
stopband attenuation	20	[dB]
sample rate	18×10^3	[Hz]

FIR filter of order $N = 70$ is applied whose design specifications are provided in Tab. 3 and whose magnitude response function is plotted in Fig. 6. Note that frequencies below the lower cut-off frequency ($\lessapprox 80$ [Hz]) of the actuator (indicated with a red dashed line in Fig. 2) are attenuated.

The magnitude response of actuator transfer function in Fig. 2 shows that frequencies above the upper cutoff frequency (≈ 1000 [Hz]) are suppressed, hence the increase of actuation frequency $f_\mathrm{a} = 1/\Delta T$ above the double of this cutoff frequency cannot significantly improve the performance of the controller. Consequently, the actuation frequency is chosen to be $f_\mathrm{a} = 2000$ [Hz]. Given that f_s is almost one order of magnitude higher than f_a, assumption $\Delta T = \kappa \Delta t$, $\kappa \in \mathbb{Z}^+$ is justified.

3 STABILITY ANALYSIS

After substitution of Eqn. (33) and Eqns. (40)–(41) into (14), the closed-loop governing equations of the full model and of models subjected to Simplifications I-II take the form of

$$\dot{\mathbf{z}}(t) = (\mathbf{A} - \mathbf{B}(t))\mathbf{z}(t) + \mathbf{B}(t)\mathbf{z}(t - \hat{\tau}) + \mathbf{E}_{j-1} + \sum_{r=r_p}^{r_p+N} \mathbf{C}_r \sum_{k=0}^{\kappa-1} \mathbf{z}(t_j + (k-r)\Delta\hat{t}) + \mathbf{F}_\mathrm{p}(t), \quad t \in \left[t_j, t_j + \Delta\hat{T}\right), \tag{42}$$

$$\mathbf{E}_j = \mathbf{E}_{j-1} + \sum_{r=r_p}^{r_p+N} \mathbf{C}_r \sum_{k=0}^{\kappa-1} \mathbf{z}(t_j + (k-r)\Delta\hat{t}), \tag{43}$$

which is a hybrid system of DDEs and difference equations (DEs) with coefficient matrices

$$\mathbf{B}(t) = H(t)\mathbf{b}\,[1\ 0\ \cdots\ 0], \quad \mathbf{C}_r = C_{r-r_\mathrm{p}}\mathbf{d}\,[0\ \cdots\ 0\ 1] \tag{44}$$

and vectors $\mathbf{E}_j = \mathbf{d}E_j$, $\mathbf{F}_\mathrm{p}(t) = \mathbf{b}F_0(t)$. By fixing the ratio between time period $\hat{\tau}$ of periodic coefficient $H(t)$ and time-period $\Delta\hat{T}$ of actuation as $\hat{\tau}/\Delta\hat{T} = \sigma/\rho$ with $\sigma, \rho \in \mathbb{Z}^+$, a dimensionless principal period $\hat{T}_\mathrm{p} = \sigma\Delta\hat{T} = \rho\hat{\tau}$ can be established. For this special case, a periodic solution of Eqns. (42)–(43) can be found. The stability of this periodic solution is then determined by variational system

$$\dot{\phi}(t) = (\mathbf{A} - \mathbf{B}(t))\phi(t) + \mathbf{B}(t)\phi(t - \hat{\tau}) + \varepsilon_{j-1} + \sum_{r=r_p}^{r_p+N} \mathbf{C}_r \sum_{k=0}^{\kappa-1} \phi(t_j + (k-r)\Delta\hat{t}), \quad t \in \left[t_j, t_j + \Delta\hat{T}\right), \tag{45}$$

$$\varepsilon_j = \varepsilon_{j-1} + \sum_{r=r_p}^{r_p+N} \mathbf{C}_r \sum_{k=0}^{\kappa-1} \phi(t_j + (k-r)\Delta\hat{t}), \tag{46}$$

where $\phi(t)$ and ε_j are the perturbation around the periodic solution. For more details and for a more rigorous treatment of similar hybrid time delay systems, see [11].

By following the same derivation process, Simplification III results in a variational system of the form

$$\dot{\phi}(t) = (\mathbf{A} - \mathbf{B}(t))\phi(t) + \mathbf{B}(t)\phi(t - \hat{\tau}) + \varepsilon_{j-1} + \sum_{r=r_p}^{r_p+N} \mathbf{C}_{3,r} \sum_{k=0}^{\kappa-1} \dot{\phi}(t_j + (k-r)\Delta\hat{t}), \quad t \in \left[t_j, t_j + \Delta\hat{T}\right), \tag{47}$$

$$\varepsilon_j = \varepsilon_{j-1} + \sum_{r=r_p}^{r_p+N} \mathbf{C}_{3,r} \sum_{k=0}^{\kappa-1} \dot{\phi}(t_j + (k-r)\Delta\hat{t}), \tag{48}$$

TABLE 4. SYSTEM PARAMETERS

Parameter	Notation	Value	Unit
modal mass	m	0.03993	[kg]
damping ratio	ζ	0.011	[1]
natural angular frequency	ω_{n}	$2\pi\times 922$	[rad/s]
tangential force coefficient	K_{t}	6×10^8	[N/m^2]
normal force coefficient	K_{n}	2×10^8	[N/m^2]
number of cutting teeth	Z	2	[1]
radial immersion ratio	a_{e}/D	0.1	[1]
sampling frequency	f_{s}	18×10^3	[Hz]
actuation frequency	f_{a}	2×10^3	[Hz]

where $\mathbf{C}_{3,r} = C_{r-r_{\mathrm{p}}}\mathbf{d}\,[0\;0\;0\;1\;0]$. The stability analysis of variational systems Eqns. (45)–(48) was carried out using the methods detailed in [11].

4 RESULTS

Under parameter values displayed in Tab. 4, results show that significant differences in SLDs can occur between the full model and its simplifications at low and high speed machining. With the increase of feedback gain G these differences are amplified. While Simplification I results in minor differences, Simplifications II-III lead to significant changes compared to the full model.

5 CONCLUSIONS

This paper dealt with the development of a new, generalized model for actively damped milling processes. The dynamics and control loop of the active damper was incorporated in addition to the so-called regenerative effect which is often the source of machine tool chatter in milling processes. It was shown that the consideration of inertial actuator and accelerometer dynamics in the model of the closed-loop system can be essential in order to obtain accurate results for stability lobe diagrams.

ACKNOWLEDGMENT

This research was supported by the National Research, Development and Innovation Office of the Hungarian Government under grant NKFI FK 124361 and by the Ministry of Human Resources of the Hungarian Government under grant ÚNKP Bolyai+ (ÚNKP-18-4-BME-193).

REFERENCES

[1] Stepan, G., 2001. “Modelling nonlinear regenerative effects in metal cutting”. *Philosophical Transactions of the Royal Society A,* ***359***, pp. 739–757.

[2] Altintas, Y., 2012. *Manufacturing Automation*. Cambridge University Press, New York.

[3] Tarng, Y. S., Kao, J. Y., and Lee, E. C., 2000. “Chatter suppression in turning operations with a tuned vibration absorber”. *Journal of Materials Processing Technology,* ***105***, pp. 55–60.

[4] Sims, N. D., 2007. “Vibration absorbers for chatter suppression: A new analytical tuning methodology”. *Journal of Sound and Vibration,* ***301***, pp. 592–607.

[5] Mei, D., Kong, T., Shih, A. J., and Chen, Z., 2009. “Magnetorheological fluid-controlled boring bar for chatter suppression”. *Journal of Materials Processing Technology,* ***209***, pp. 1861–1870.

[6] Zatarain, M., Bediaga, I., Munoa, J., and Lizarralde, R., 2008. “Stability of milling processes with continuous spindle speed variation: Analysis in the frequency and time domains, and experimental correlation”. *CIRP Annals – Manufacturing Technology,* ***57***, pp. 379–384.

[7] van Dijk, N. J. M., van de Wouw, N., Doppenberg, E. J. J., Oosterling, H. A. J., and Nijmeijer, H., 2012. “Robust active chatter control in the high–speed milling process”. *IEEE Transactions on Control Systems Technology,* ***20(4)***, pp. 901–917.

[8] Munoa, J., Mancisidor, I., Loix, N., Uriarte, L. G., Barcena, R., and Zatarain, M., 2013. “Chatter suppression in ram type travelling column milling machines using a biaxial inertial actuator”. *CIRP Annals – Manufacturing Technology,* ***62***, pp. 407–410.

[9] Lehotzky, D., and Insperger, T., 2012. “Stability of turning processes subjected to digital PD control”. *Periodica Polytechnica Mechanical Engineering,* ***56***(1), pp. 33–42.

[10] Lehotzky, D., and Insperger, T., 2014. “Stabilizability diagram for turning processes subjected to digital PD control”. *International Journal of Dynamics and Control,* ***2***, pp. 46–54.

[11] Lehotzky, D., Insperger, T., and Stepan, G., 2018. “Numerical methods for the stability of time-periodic hybrid time-delay systems with applications”. *Applied Mathematical Modelling,* ***57***, pp. 142–162.

[12] Preumont, A., 2011. *Vibration Control of Active Structures*, 3 ed. Springer, Berlin.

[13] Camperi, S., Ghanchi-Tehrani, M., Zilletti, M., and Elliott, S. J., 2016. “Active vibration control of an inertial actuator subject to broadband excitation”. *Journal of Physics: Conference Series,* ***744***(012038), pp. 1–10.

[14] Huyanan, S., and Sims, N. D., 2007. “Vibration control strategies for proof–mass actuators”. *Journal of Sound and Vibration,* ***13(12)***, pp. 1785–1806.

[15] Bilbao-Guillerna, A., Azpeitia, I., Luyckx, S., Loix, N., and Munoa, J., 2012. "Low frequency chatter suppression using an inertial actuator". In 9th CIRP International Conference on High Speed Machining, San Sebastian, Spain, pp. 61–66.

[16] Mancisidor, I., Munoa, J., Barcena, R., Beudaert, X., and Zatarain, M., 2015. "Coupled model for simulating active inertial actuators in milling processes". *International Journal of Advanced Manufacturing Technology,* ***77***, pp. 581–595.

[17] Mancisidor, I., Munoa, J., and Barcena, R., 2014. "Optimal control laws for chatter suppression using inertial actuator in milling processes". In 11th International Conference on High Speed Machining (HSM2014), Prague, Czech Republic.

[18] Yu, J. C., and Lan, C. B., 2001. "System modeling of microaccelerometer using piezoelectric thin films". *Sensors and Actuators A,* ***88***, pp. 178–186.

[19] Dombovari, Z., Iglesias, A., Zatarain, M., and Insperger, T., 2011. "Prediction of multiple dominant chatter frequencies in milling processes". *International Journal of Machine Tools and Manufacture,* ***51***, pp. 457–464.

[20] Stepan, G., Dombovari, Z., and Munoa, J., 2011. "Identification of cutting force characteristics based on chatter experiments". *CIRP Annals – Manufacturing Technology,* ***60***, pp. 113–116.

[21] Long, X. H., Balachandran, B., and Mann, B. P., 2007. "Dynamics of milling processes with variable time delays". *Nonlinear Dynamics,* ***47***, pp. 49–63.

[22] Faassen, R. P., van de Wouw, N., Nijmeijer, H., and Oosterling, J. A., 2006. "An improved tool path model including periodic delay for chatter prediction in milling". *Journal of Computational and Nonlinear Dynamics,* ***2(2)***, pp. 167–179.

[23] Bachrathy, D., Stepan, G., and Turi, J., 2011. "State dependent regenerative effect in milling processes". *Journal of Computational and Nonlinear Dynamics,* ***6(4)***(041002), pp. 1–9.

[24] Insperger, T., and Stepan, G., 2011. *Semi–discretization for time–delay systems*. Springer, New York.